Solution of the Euler Equations in Three Dimensional Complex Geometries Using a Fully Unfactored Method

M. Woodgate, K. Badcock, F. Cantariti, and B. Richards
Aerospace Engineering Report 9907

Aerospace Engineering Department, University of Glasgow, Glasgow G12 8QQ, U.K.

Abstract

An unfactored implicit time-marching method for the solution of the three dimensional Euler equations on multiblock curvilinear grids is presented. For robustness the convective terms are discretised using an upwind TVD scheme. The linear system arising from each implicit time step is solved using a Krylov subspace method with preconditioning based on an block incomplete lower-upper (BILU(0)) factorisation. Results are shown for the ONERA M6 wing, a wing/body configuration and the NLR-F5 wing with launcher and missile. It was found that the simulation cost is relatively independent of the number of blocks used and their orientation. Comparison is made with experiment where available and good agreement is obtained.

1 Introduction

Due to the availability of increased computing power and the advances in numerical methods, computational fluid dynamics (CFD), is becoming an important tool for analysing the aerodynamics of aircraft [12]. Opportunities are opening up for the use of CFD to reduce design cycle costs, evaluate experimental inaccuracies (eg tunnel interference) and provide high resolution information to aid the understanding of flow physics. The most demanding problems for aircraft are experienced in the transonic and supersonic regimes where the minimum level of modelling to satisfactorally model shock waves is the Euler equations. Due to the high Reynolds' numbers often encountered in practical aircraft, rotorcraft and missile flight, and the interest in maintaining attached flow, the modelling of viscous effects is often unnecessary. This is helpful due to the increased cost of resolving turbulent boundary layers.

Euler solvers for complex aircraft shapes have been used for a number of years. Geometric complexity is tackled through the use of either unstructured or block structured grids. The former have the advantage of grid generation with less human intervention. However, flow codes on unstructured grids require more memory and are generally less efficient. For one-off simulation the large cost of the grid generation stage means that unstructured grids are normally preferred for Euler calculations. However, in multi-disciplinary worksuch as optimisation, where repetitive flow simulations are required, the emphasis shifts to flow code efficiency and block structured grids are attractive.

The current report describes the development of an implicit method for solving the three dimensional steady state Euler equations. This work builds on developments in two dimensions. The features of the method are an iterative solution [6] of an unfactored linear system for the flow updates [3], approximate Jacobian matrices [8] and a preconditioning strategy designed to provide good parallel performance [4]. Applications of the method for steady state problems include for aerofoil flows [3] [8], multielement aerofoils [2], axisymmetric slender body shapes [1] and shock wave reflections in jets [5].

The report continues with a description of the Euler equations, followed by the numerical method. Results are then presented for the ONERA M6 wing to show the influence of the grid density, number of blocks, linear solver convergence level and block orientation on the method performance. The code is then demonstrated on a wing body configuration and the NLR F5 wing with launcher and missile. Comparison with experimental data is made where available and computing times are given to illustrate the performance of the method.

2 Three-Dimensional Euler Equations

The three-dimensional Cartesian Euler equations can be written in conservative form as

$$\frac{\partial \mathbf{W}}{\partial t} + \frac{\partial \mathbf{F}}{\partial x} + \frac{\partial \mathbf{G}}{\partial y} + \frac{\partial \mathbf{H}}{\partial z} = 0 \qquad (1)$$

where $\mathbf{W} = (\rho, \rho u, \rho v, \rho w, \rho E)^T$ denotes the vector of conservative variables. The flux vectors $\mathbf{F}$, $\mathbf{G}$ and $\mathbf{H}$ are,

$$\mathbf{F} = \begin{pmatrix} \rho u \\ \rho u^2 + p \\ \rho uv \\ \rho uw \\ u(\rho E + p) \end{pmatrix},$$

$$\mathbf{G} = \begin{pmatrix} \rho v \\ \rho uv \\ \rho v^2 + p \\ \rho vw \\ v(\rho E + p) \end{pmatrix},$$

$$\mathbf{H} = \begin{pmatrix} \rho w \\ \rho uw \\ \rho vw \\ \rho w^2 + p \\ w(\rho E + p) \end{pmatrix}.$$

In the above ρ, u, v, w, p and ρE denote the density, the three Cartesian components of the velocity, the pressure and the specific total energy respectively.

3 Numerical Method

3.1 Spatial Discretisation

The Euler equations are discretised on curvilinear multi-block body conforming grids using a cell-centred finite volume method which converts the partial differential equations of (1) into a set of ordinary differential equations which can be written as

$$\frac{d}{dt}(V_{i,j,k}\mathbf{W}_{i,j,k}) = -\mathbf{R}_{i,j,k}(\mathbf{W}). \quad (2)$$

The convective terms are discretised using Osher's upwind scheme [7] for its robustness, accuracy and stability properties. MUSCL variable extrapolation is used to provide second-order accuracy with the Van Albada limiter to prevent spurious oscillations around shock waves.

3.2 Implicit Unfactored method

The implicit time marching scheme for equation (2) is given by

$$\frac{\mathbf{W}^{n+1}_{i,j,k} - \mathbf{W}^{n}_{i,j,k}}{\Delta t} = -\frac{1}{V_{i,j,k}}\mathbf{R}_{i,j,k}(\mathbf{W}^{n+1}) \quad (3)$$

where the superscript $n+1$ denotes the time level $(n+1) \times \Delta t$. In order to be able to solve equation (3) more easily the term $\mathbf{R}_{i,j,k}(\mathbf{W}^{n+1})$ is linearised with respect to time:

$$\mathbf{R}_{i,j,k}(\mathbf{W}^{n+1}) \approx \mathbf{R}_{i,j,k}(\mathbf{W}^{n}) + \frac{\partial \mathbf{R}_{i,j,k}}{\partial \mathbf{W}_{i,j,k}}\Delta \mathbf{W}_{i,j,k} \quad (4)$$

where $\Delta \mathbf{W}_{i,j,k} = \mathbf{W}^{n+1}_{i,j,k} - \mathbf{W}^{n}_{i,j,k}$. This leads to the following linear system

$$\left[\frac{V_{i,j,k}}{\Delta t}\mathbf{I} + \frac{\partial \mathbf{R}_{i,j,k}}{\partial \mathbf{W}_{i,j,k}}\right]\Delta \mathbf{W}_{i,j,k} = -\mathbf{R}_{i,j,k}(\mathbf{W}^{n}). \quad (5)$$

In the present work, the left hand side of equation (5) is approximated with first order Jacobians as in [8]. This nearly halves the number of terms in the matrix from 325 per cell to 175 which is essential as 3D problems can easily have over a million cells. Initial results have indicated that the present method requires 1 MB of memory per 550 nodes. The right hand side of (5) is not changed to maintain second order spatial accuracy. A Krylov subspace algorithm is used to solve the linear system of equation and is preconditioned using a Block Incomplete Lower-Upper factorisation which has the same sparsity pattern as the Jacobian matrix (BILU(0)). Furthermore, the BILU(0) factorisation is decoupled between blocks to improve parallel efficiency. This approach does not seem to have a major impact on the effectiveness of the preconditioner as the number of blocks increases in 2D [9]. The block orientation in the present method is to align the ξ direction with the flow, the η direction is the direction normal to any surface and ζ is the remaining direction, usually the spanwise or cylindrical direction wherever possible.

4 Computational Results

4.1 Results for the ONERA M6 Wing

The first test case considered is the flow around the ONERA M6 wing at a freestream Mach number of 0.84 and an angle of attack of 3.06^o. A C-O grid was generated containing $257 \times 65 \times 97$ points, with 193 points wrapped around the wing in the flow direction and 65 points in the direction normal to the wing. In the spanwise direction, there are 73 points on the wing and 25 points wrapped around half of the tip. The farfield boundary is situated approximately 11 chords from the wing. From this fine grid, two grid levels were extracted by removing every other point each time. An overview of the flow features on the wing upper surface is shown in Figures 1 and 2 for the medium and fine grid, respectively. There is little difference between the two sets of results, except that the shock wave is captured more cleanly on the fine grid, as expected. The lambda shape of the shock wave is also observed experimentally [10]. The predicted pressure coefficient distributions around the wing agree well with the experimental data for the medium and fine grid (see Figure 3). In particular, the pressure coefficient on the lower surface is accurately predicted, as for the suction levels upstream of the first shock on the upper surface.

Because the geometric definition of this problem is relatively simple, this test case was also used to evaluate the performance of the present method.

4.1.1 Grid Density Study

A comparison of the pressure distributions for the three different grids is shown in Figure 3. It can be seen that the coarse grid is not sufficient to resolve the flow features, but differences for the medium and fine grids are small and are limited to the shock waves. Hence, it seems that the $129 \times 33 \times 49$ medium grid is sufficient to resolve the flow features for that case. This is confirmed in Table 1 where the predicted lift and drag coefficients for the medium and fine grids are within 1% and 10%, respectively. However, the coarse grid calculation under-predicts the lift coefficient by 6% and grossly over-predicts the drag coefficient by 60%. The time in work units, where one work unit is the the time taken to do one explicit iteration, as well as CPU time both scale very well as the problem size is increased. For both the medium and fine grids interpolated solutions from the lower grid are used as the initial guess.

4.1.2 Influence of the Linear System Convergence Level

Next, the influence of the convergence level of the linear system arising at each implicit time step is examined. Its convergence level is measured by the ratio of the L2 norm of the current residual of the linear system with the L2 norm of the initial residual. The influence of that ratio is shown in Table 2. As expected, a more accurate resolution of the linear system requires more iterative steps to solve the system, but leads to fewer implicit time steps to converge the governing equations. Since the Jacobian matrix is approximated the update $\delta \mathbf{W}_{i,j,k}$ has itself been approximated and so the benefit of calculating this approximation accurately has less effect on the number of implicit iterations as the convergence level is reduced. Overall, the total runtime of the solver remains fairly constant up to a ratio of the L2 norm to the initial value of 0.01. Hence, this value was selected for all the calculations done in the present paper.

4.1.3 Influence of the Number of Blocks

This section examines the influence of the number of blocks on the convergence. Since an approximation is introduced in the BILU(0) factorisation used for the preconditioner by decoupling it between blocks, it is important to ensure that the number of blocks has little influence on the numerical method. This is confirmed in Table 3 where the overall runtime of the flow solver remains fairly constant for a number of blocks varying between 12 and 64. It is important to note that the present case is a difficult one for the block-decoupled preconditioner since non-linear flow feature such as shock waves are present across several blocks yet the solution is invariant to the number of blocks used.

4.1.4 Influence of the Block Orientation

This final section for the ONERA M6 wing examines the influence of the block orientation on the present method. The use of different block orientations reorders the equations within that block but the 5 variables for each cell remain together. Figure 4 shows how the C-O mesh topology looks in the global coordinate system and conforms to the default block orientation outlined in Section 3.2. It can be seen from Table 4 that the linear solver is invariant to the orientation of block when numbered from a same corner. The default configuration, row one, is no better nor worst than any other possible configuration. This means that the linear solver plus BILU(0) preconditioner has no prefered direction in the numbering of the equations for this case.

5 Demonstration Results

5.1 Results for the GARTEUR AG24 Wing/body

For this case, the computational grid is made of 22 blocks and contains a total of 409600 cells. The preferred block orientation is used, with the ξ direction running along the body from apex to the downstream boundary, the η direction corresponds to the direction normal to the body and the ζ direction goes around the body from the symmetry plane on the upper surface to the symmetry plane on the lower surface. Two flow conditions were considered at an angle of attack of 0^o and 8^o, both at a Mach number of 2.5. Although a quarter of the wing/body configuration could have been used for the 0^o incidence case, half configuration was used for simplicity. A typical run took 45 minutes on 6 processors on a cluster of Pentium Pro machines to reduce the L2 norm of the residual by 8 orders.

The pressure contours on the wing/body as well as on the upper and lower surfaces symmetry planes are shown in Figures 5 and 6 for the two flow conditions. In Figure 5, it can be seen that the flow is symmetrical and that all the shock and expansion waves are cleanly captured. For the 8^o case, stronger shock and expansion waves are observed on the windward side of the body. Also, on the leeward side of the horizontal wing, there exists a very low pressure region.

5.2 Results for the NLR-F5 Wing with Launcher and Missile

The final test case is for the NLR-F5 wing with launcher and missile at the tip of the wing. The computational grid is split into 290 blocks and contains 169448 cells. The flow conditions for this problem are an angle of attack of 0^o and a Mach number of 0.897. This is a challenging problem for the numerical method because of the geometrical complexity of the problem, hence the large

number of blocks required, because of the large variation in the size of the blocks (the largest contains 5520 cells while the smallest has only 32 cells) and because of the complexity of the flow field. The runtime of the code was 2 hours and 15 minutes on 4 processors on a cluster of Pentium Pro machines to reduce the L2 norm of the residual by 5 orders. An overview of the flow on the wing, launcher and missile is shown in Figures 7 and 8 for the upper and lower surfaces, respectively. It can be seen that a shock wave is present on the wing upper surface from root to tip.

The predicted pressure coefficient distributions are compared with the experimental data [11] in Figure 9. It can can be seen that the agreement on the lower surface between experiment and calculation is good. However, there are some discrepancies on the upper surface. Towards the root of the wing, a shock wave is predicted whereas no such flow feature exists in the experiment. This is due to the absence of viscous effects in the numerical method which will tend to over-predict the suction levels on the wing. Also, the pressure coefficient in the middle of the wing upper surface is close to its critical sonic value of 0.194 for the present freestream Mach number. Therefore, a slight over-prediction of the pressure levels will have a large influence on the presence or absence of a shock wave. Towards the center of the wing, stations $\eta = 0.641$ to $\eta = 0.875$, a shock exists in the experiment. However, the calculated one is situated too far downstream, by about 10% chord, and its strength is over-predicted. This leads to a pressure coefficient bubble which is too large at the last station next to the launcher.

6 Conclusion

An unfactored implicit time-marching method for solving the three dimensional Euler equations has been presented in this paper. Results were shown for the ONERA M6 wing, a wing/body configuration and the NLR-F5 wing with launcher and missile. The ONERA M6 wing was also used to evaluate the characteristics of the present method. It was found that the solution procedure is relatively independent on the number of blocks and their orientation. Good results were obtained for all cases considered.

Acknowledgements

The authors would like to thank Trevor Birch (DERA) and Michael Henshaw (BAe) for making available the grids for the GARTEUR AG24 Wing/body and NLR-F5 Wing with launcher and missile, respectively. Also, this work has been partially supported BAe contract (SP050104458), Defence and Evaluation Research Agency (DERA) contract FRNI c/107 and EPSRC (GR/K55455).

References

[1] B.J.Gribben, K.J.Badcock, and B.E.Richards, "Application of PMB2D to axisymmetric flows", Aerospace Engineering Report, 12, Glasgow University, Glasgow, UK, 1998.

[2] B.J.Gribben, "Progress Report: Application of the multiblock method in Computational Aerodynamics", Aerospace Engineering Report, 21, Glasgow University, Glasgow, UK, 1996.

[3] K.J.Badcock and S.Porter and B.E.Richards, "Unfactored Multiblock Methods:Part I Initial Method Development", Aerospace Engineering Report, 11, Glasgow University, Glasgow, UK, 1995.

[4] K.J.Badcock, W.S.McMillan, M.A.Woodgate, B.Gribben, S.Porter, and B.E.Richards, "Integration of an implicit multiblock code into a workstation cluster environment", in *Parallel CFD 96*, p. 408. Capri, Italy, 1996.

[5] B.J. Gribben, K.J. Badcock and B.E. Richards. "Shock Reflection Hysteresis in an Underexpanded Jet: a CFD Study". *University of Glasgow, Aero Report 9808*, 1998.

[6] K.J.Badcock, X.Xu and L.Dubuc and B.E.Richards, "Preconditioners for high speed flows in aerospace engineering", *Numerical Methods for Fluid Dynamics V*,Institute for Computational Fluid Dynamics, Oxford, pp287–294,1996

[7] Osher, S. and Chakravarthy, S., "Upwind Schemes and Boundary Conditions with Applications to Euler Equations in General Geometries", *Journal of Computational Physics*, Vol. 50, pp 447-481, 1983.

[8] Cantariti, F., Dubuc, L., Gribben, B., Woodgate, M., Badcock, K. and Richards, B., "Approximate Jacobians for the Solution of the Euler and Navier-Stokes Equations", Department of Aerospace Engineering, Technical Report 97-05, 1997. Also, http://www.aero.gla.ac.uk/Research/CFD/Index.html under publications/codes.

[9] Badcock, K., McMillan, W., Woodgate, M., Gribben, B., Porter, S. and Richards, B., "Integration of an Implicit Multiblock Code into a Workstation Cluster Environment", *Parallel Computational Fluid Dynamics: Algorithms and Results using Advanced Computers*, P. Schiano *et al.* (Eds.), Elsevier Science B.V. Amsterdam, pp 408-415, 1996.

[10] Schmitt, V. and Charpin, F., "Pressure Distributions on the ONERA-M6-Wing at Transonic Mach Numbers", in "Experimental Data Base for Computer Program Assessment", AGARD-AR-138, 1979.

[11] Tijdeman, H. *et al.*, "Transonic Wind Tunnel Tests on an Oscillating Wing with External Store. Part III: The Wing with Tipstore", NLR TR 78106 U, 1978.

[12] Jameson, A. , "The present status, challenges and future developments in computational fluid dynamics", *AGARD symposium on Progress and Challenges in CFD Methods and Algorithms*, Seville, Spain, October 1995.

Table 1: Integrated loads
ONERA M6 wing, $M_\infty = 0.84$, $\alpha = 3.06^o$

Grid	C_L	C_D	Work Units	CPU Minutes
fine	0.2913	0.00116	790	690
medium	0.2886	0.00127	709	80
coarse	0.2752	0.00188	560	8.4

Table 2: Influence of linear system convergence level
ONERA M6 wing, $M_\infty = 0.84$, $\alpha = 3.06^o$

Reduction of the initial residual by	Number of implicit iterations	Average number of steps to solve linear system	Total number of Work Units
0.05	306	7.1	2150
0.01	230	9.5	2200
0.005	226	11.2	2400
0.001	212	13.7	2700

Table 3: Influence of number of blocks
ONERA M6 wing, $M_\infty = 0.84$, $\alpha = 3.06^o$

Number of blocks	Number of implicit iterations	Total number of Work Units
12	230	2200
24	240	2240
32	246	2400
64	248	2340

Table 4: Influence of the block orientation
ONERA M6 wing, $M_\infty = 0.84$, $\alpha = 3.06^o$

Block orientation	Number of implicit iterations	Total number of Work Units
(ξ,η,ζ)	230	2200
(ζ,ξ,η)	230	2200
(η,ζ,ξ)	230	2200
(ξ,ζ,η)	230	2200

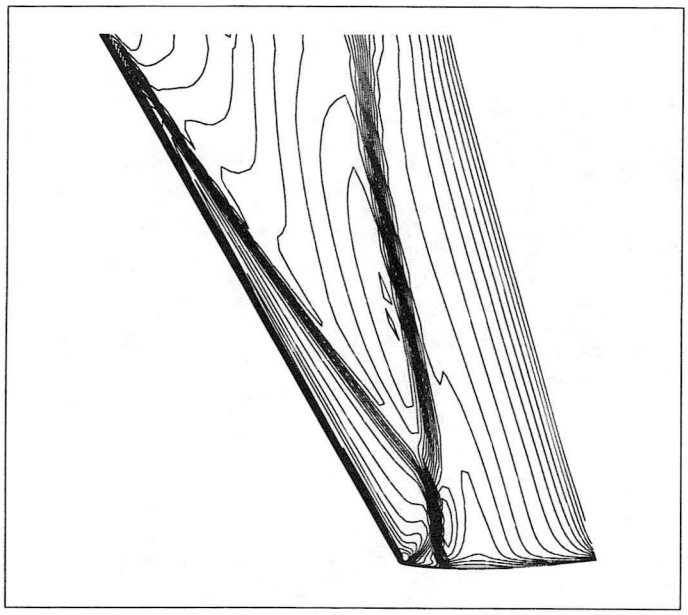

Figure 1: Pressure contours for the ONERA M6 Wing
Medium grid, $M_\infty = 0.84$, $\alpha = 3.06^o$

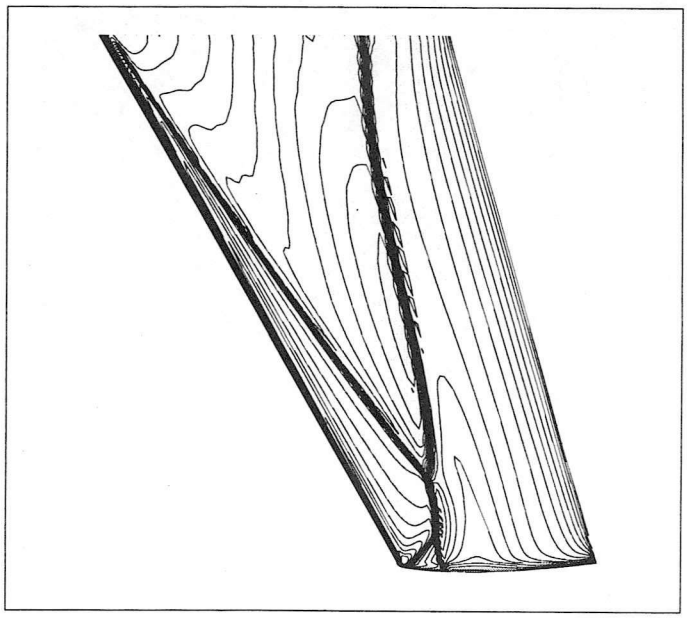

Figure 2: Pressure contours for the ONERA M6 Wing
Fine grid, $M_\infty = 0.84$, $\alpha = 3.06^o$

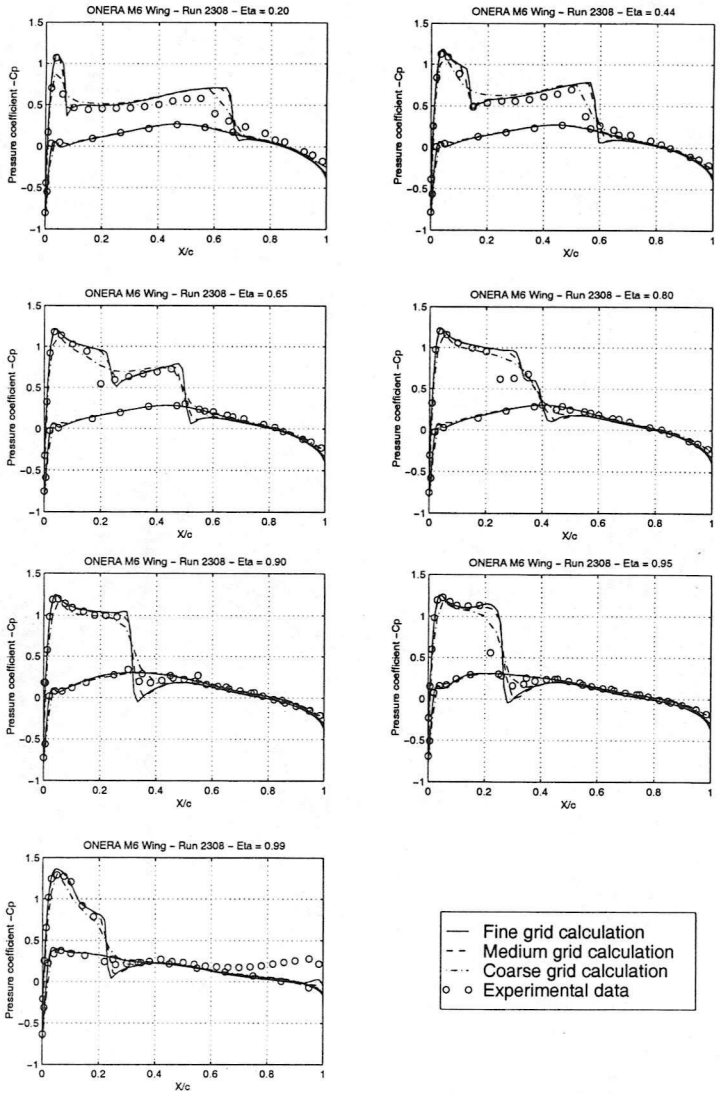

Figure 3: Pressure distribution for different grid densities
ONERA M6 Wing, $M_\infty = 0.84$, $\alpha = 3.06^o$

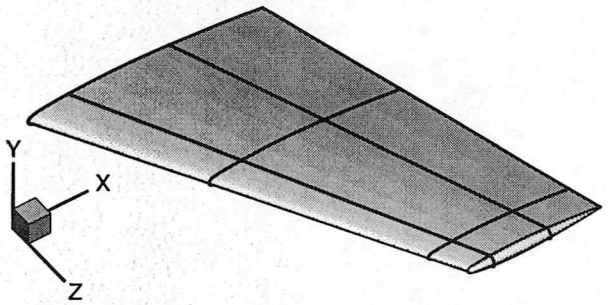

Figure 4: Global coordinate system for the C-O ONERA M6 Wing mesh

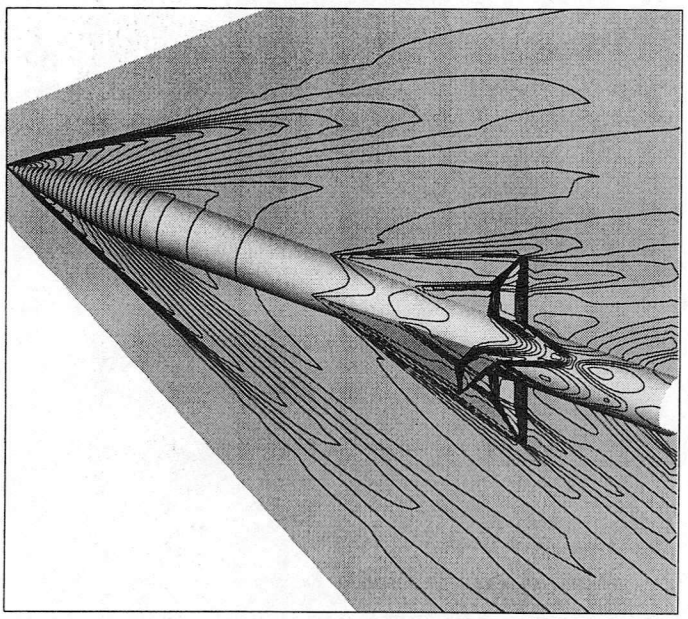

Figure 5: Pressure contours for the Wing/body configuration
$M_\infty = 2.5, \alpha = 0^o$

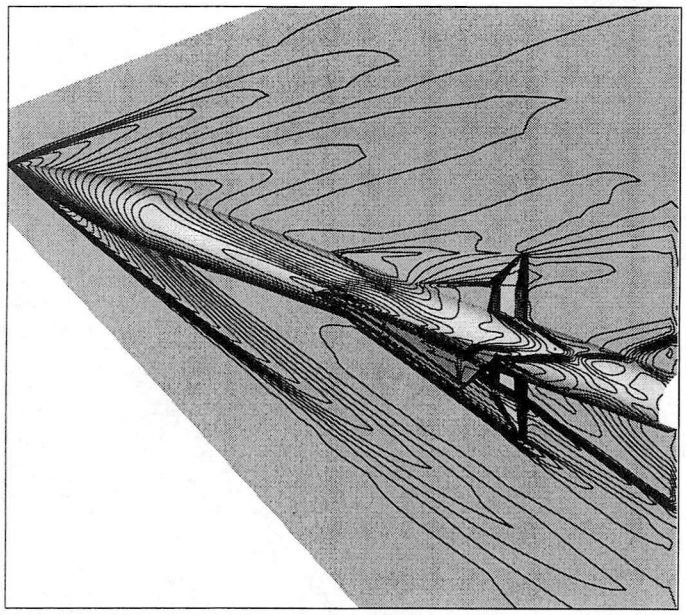

Figure 6: Pressure contours for the Wing/body configuration
$M_\infty = 2.5, \alpha = 8^o$

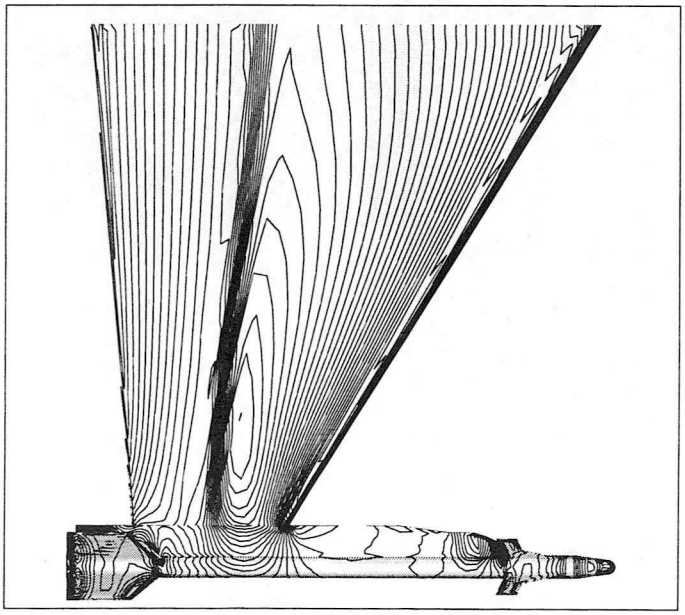

Figure 7: Pressure contours for F5 Wing with launcher and missile
Upper Surface, $M_\infty = 0.897, \alpha = 0^o$

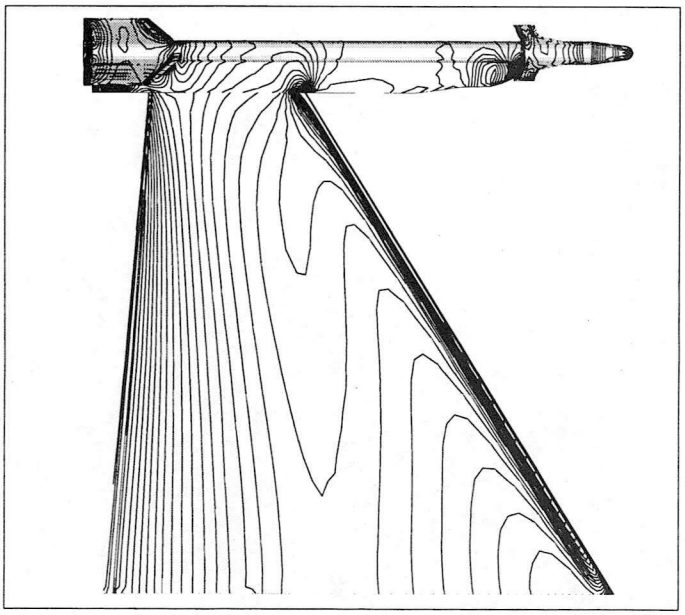

Figure 8: Pressure contours for F5 Wing with launcher and missile
Lower Surface, $M_\infty = 0.897$, $\alpha = 0^o$

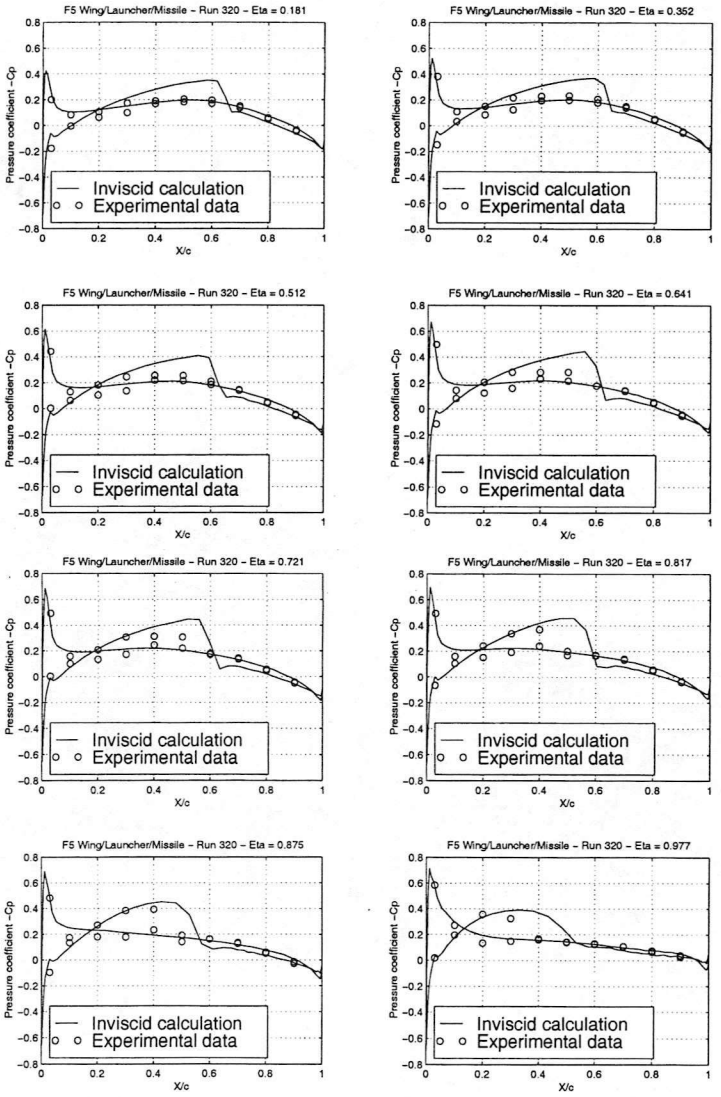

Figure 9: Pressure distribution for F5 Wing with launcher and missile
$M_\infty = 0.897, \alpha = 0^o$